Structure and reactivity of hydroxypropylphosphonic acid epoxidase in fosfomycin biosynthesis by a cation- and flavin-dependent mechanism

Karen McLuskey[†‡], Scott Cameron[†‡], Friedrich Hammerschmidt[§], and William N. Hunter[†¶]

[†]Division of Biological Chemistry and Molecular Microbiology, School of Life Sciences, University of Dundee, Dundee DD1 5EH, United Kingdom; and [§]Institute of Organic Chemistry, University of Vienna, A-1090 Vienna, Austria

Edited by David R. Davies, National Institutes of Health, Bethesda, MD, and approved August 19, 2005 (received for review May 25, 2005)

The biosynthesis of fosfomycin, an oxirane antibiotic in clinical use, involves a unique epoxidation catalyzed by (*S*)-2-hydroxypropylphosphonic acid epoxidase (HPPE). The reaction is essentially dehydrogenation of a secondary alcohol. A high-resolution crystallographic analysis reveals that the HPPE subunit displays a two-domain combination. The C-terminal or catalytic domain has the cupin fold that binds a divalent cation, whereas the N-terminal domain carries a helix–turn–helix motif with putative DNA-binding helices positioned 34 Å apart. The structure of HPPE serves as a model for numerous proteins, of ill-defined function, predicted to be transcription factors but carrying a cupin domain at the C terminus. Structure–reactivity analyses reveal conformational changes near the catalytic center driven by the presence or absence of ligand, that HPPE is a Zn^{2+}/Fe^{2+}-dependent epoxidase, proof that flavin mononucleotide is required for catalysis, and allow us to propose a simple mechanism that is compatible with previous experimental data. The participation of the redox inert Zn^{2+} in the mechanism is surprising and indicates that Lewis acid properties of the metal ions are sufficient to polarize the substrate and, aided by flavin mononucleotide reduction, facilitate the epoxidation.

enzyme | epoxidation | iron | zinc

Fosfomycin, *cis*-(1*R*,2*S*)-epoxypropylphosphonic acid, an oxirane antibiotic in clinical use, is a clinically important antibiotic produced as a secondary metabolite by various *Streptomycetes* and *Pseudomonas* species (1–3). This relatively simple molecule is one of a growing family of natural products that contain a C—P bond; these include compounds of commercial and medical importance such as herbicides (phosphinothricin and bialaphos) and the antimalarial drug fosmidomycin (4, 5). Fosfomycin acts as an analogue of phosphoenolpyruvate and forms a covalent bond with the active site cysteine residue of UDP-GlcNAc-3-O-enolpyruvyltransferase, a key enzyme of peptidoglycan synthesis (6). The biosynthesis of the drug involves a unique epoxidation by dehydrogenation of the secondary alcohol (*S*)-2-hydroxypropylphosphonic acid (Fig. 1 and refs. 7–9).

Natural epoxides are generally formed via oxidation of alkenes by α-ketoglutarate-dependent nonheme Fe-dependent monooxygenases (10, 11) or by heme-dependent cytochrome P450 enzymes (12). Enzymes are reliant on the redox properties of Fe^{2+} for catalysis. The enzyme (*S*)-2-hydroxypropylphosphonic acid epoxidase (HPPE), encoded by the *fom4* gene of *Streptomyces wedmorensis* (3), is distinct because neither does it depend on α-ketoglutarate nor is it a cytochrome P450-type of epoxidase. HPPE has been described as a nonheme redox active Fe-dependent enzyme (8) reported to show oxygenase activity, via putative iron-oxo or hydroperoxo intermediates by the formation of a bidentate Fe^{3+}–catecholate complex (9).

We made the surprising observation that purified recombinant HPPE does not contain Fe^{2+}, yet it retains activity. The protein is in fact a mixture of mainly apo and some Zn^{2+}-containing enzyme. Crystal structures of holoenzyme (HPPE-Zn) and the complex with fosfomycin (HPPE-Fos) were determined and reveal a two-domain combination and Zn^{2+} in the active site. Because no Zn^{2+}/Fe^{2+}-dependent epoxidase has been characterized that led us to investigate the biological significance and role of the metal ions in the enzyme mechanism. We show that recombinant HPPE is active when reconstituted with Zn^{2+} or Fe^{2+} and reliant on flavin mononucleotide (FMN). A straightforward epoxidase mechanism is proposed that depends on the Lewis acid properties of divalent cations and the redox properties of FMN.

Experimental Procedures

Sample Preparation. Purification and crystallization of recombinant *S. wedmorensis* HPPE in the presence of $ZnCl_2$ (HPPE-Zn) followed published methods (13). Experimental phases were obtained by a single-wavelength anomalous dispersion experiment on a derivative (HPPE-Hg) obtained by incubating HPPE (30 mg·ml^{-1} in 20 mM Tris·HCl, pH 7.9/50 mM NaCl) on ice for 30 min with 1 mM *p*-chloromercuribenzoic acid before crystallization.

Data Collection and Processing. Crystals were cryoprotected for 30 sec in 3 M Li_2SO_4 then flash-cooled to −173°C in a stream of nitrogen gas. An HPPE-Zn–fosfomycin complex (HPPE-Fos) was obtained by soaking a crystal in 3 M fosfomycin for 20 sec before flash cooling. Three data sets from isomorphous hexagonal crystals are reported (Table 1). Data to 1.9- and 2.5-Å resolution were obtained for HPPE-Hg and HPPE-Fos, respectively, in-house on a Rigaku (Tokyo) Micromax 007 rotating anode generator with an *R* axis IV^{2+} detector. High-resolution data for HPPE-Zn were collected on station BM14 at the European Synchrotron Radiation Facility by using a Mar-Research (Hamburg) Marmosaic detector. Data were processed with DENZO/SCALEPACK (14) and MOSFLM/CCP4 programs (15).

Structure Solution and Refinement. Initial phases were derived (16) by the single-wavelength anomalous dispersion approach exploiting the highly redundant data measured from HPPE-Hg (Table 1). The asymmetric unit contains two subunits, A and B, and each carries a single cysteine (Cys-107). Two Hg^{2+} positions, each with occupancy of 0.5, coordinate the cysteines. Phases were calculated to 3-Å resolution with a figure of merit (FOM) of 0.38. Solvent flattening (16) and phase extension to 1.9 Å gave a FOM of 0.43 and an electron density map of high quality in

This paper was submitted directly (Track II) to the PNAS office.

Freely available online through the PNAS open access option.

Abbreviations: FOM, figure of merit; HPP, (*S*)-2-hydroxypropylphosphinic acid; HPPE, HPP epoxidase; HTH, helix–turn–helix; PDB, Protein Data Bank; HPPE-Fos, HPPE-Zn–fosfomycin complex.

Data deposition: The atomic coordinates and structure factors have been deposited in the Protein Data Bank, www.pdb.org (PDB ID codes 2BNM, 2BNN, and 2BNO).

[‡]K.M. and S.C. contributed equally to this work.

[¶]To whom correspondence should be addressed. E-mail: w.n.hunter@dundee.ac.uk.

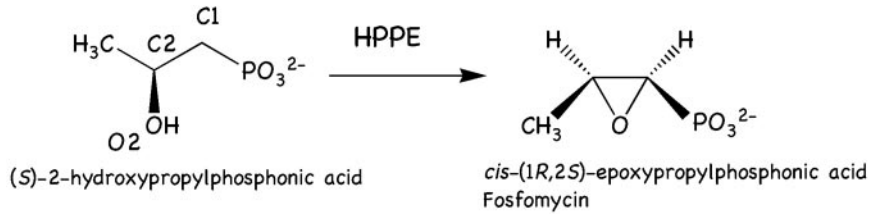

Fig. 1. The chemical reaction catalyzed by HPPE.

space group $P6_522$. An initial model, 358 of a possible 396 residues, was constructed (17). Cycles of interactive model building and refinement using O (18) and REFMAC (19) were carried out with 5% of the data set aside for the calculation of R_{free}. Subunits were treated independently, and a bulk solvent correction was applied. The inclusion of water and sulfate and metal ions completed this model. Refinement of the HPPE-Fos and HPPE-Zn structures was initiated by rigid-body refinement followed by rounds of electron and difference density map inspection, model manipulation, addition of water molecules, sulfates, and ligand/metal ion assignment. The refined model of HPPE-Zn comprises residues 5–198 for subunits A and B. The structure of HPPE-Fos is less complete, with disorder of residues 97–101 in subunit B. Multiple conformations for 50 residues in HPPE-Zn and 14 in HPPE-Fos were identified. All residues are in allowed regions of a Ramachandran plot, and statistics are given in Table 1.

Enzyme Assay. HPPE activity was investigated by a disk diffusion bioautography assay, which monitors inhibition of bacterial growth due to production of the enzyme product (8). This is a standard assay for enzyme activity linked to antibiotic production. Full details are provided as supporting information, which is published on the PNAS web site, and only a brief description is given here. Two sets of experiments were carried out, first to investigate the necessary requirements for enzyme activity and second, to quantify substrate production. Disks were set up by using the fosfomycin-sensitive strain *E. coli*-K12 and HPP. The initial assay mixture contained 10.5 mM HPP, 82 μM HPPE, 21.8 mM NADH, and 120 μM FMN buffered in 20 mM Tris·HCl, pH 7.9/50 mM NaCl. Individual components were removed to investigate their requirement for activity, whereas 2 mg·ml^{-1} fosfomycin provided a positive control. Subsequently, HPPE was stripped of divalent cations by incubation with 10 mM EDTA for 2 hr followed by extensive dialysis against the assay buffer. The apoprotein was incubated with 10 mM $NiCl_2$, $ZnCl_2$, or $Fe(NH_4)_2(SO_4)_2$ and disk diffusion assays repeated with the reconstituted samples. Next, to quantify enzyme productivity, the assays were repeated in triplicate with four samples, (*i*) HPPE as purified from the bacterial expression system, (*ii*) apo-HPPE after EDTA treatment, (*iii*) Fe^{2+}, and (*iv*) Zn^{2+} reconstituted enzymes at concentrations of 20, 40, 80, 160, 320, and 500 μM. Positive (fosfomycin) and negative (lacking HPP and HPPE) control experiments were carried out in parallel. An additional series of assays using defined amounts of fosfomycin (nine different quantities in the range 0.1–8.0 μg) provided a direct measure of the zone of inhibition and, by extrapolation, the quantity of antibiotic produced by the different enzyme samples at varying concentrations.

Isothermal Titration Calorimetry. The association of HPPE and FMN was examined by using a VP-Isothermal Titration Calorimeter and ORIGIN, Ver. 7, software (Microcal, Northampton, MA). HPPE was dialyzed into 10 mM Tris·HCl, pH 7.9/50 mM NaCl and concentrated to 100 μM. FMN was dissolved to 1 mM in the same buffer, and 25 injections of 10 nmol were made. After integration, the determined heat of dilution was subtracted from the heat of reaction.

Metal Ion Identification. Atomic absorption spectroscopy on HPPE at a concentration of 280 nM in 20 mM Tris·HCl, pH

Table 1. Crystallographic statistics

Structure	HPPE-Zn	HPPE-Hg	HPPE-Fos
Unit cell lengths *a, c*, Å	86.4, 221.9	86.4, 221.4	85.6, 218.0
Wavelength, Å	1.2710	1.5418	1.5418
Resolution range, Å	30–1.7	30–1.9	30–2.5
No. of measurements	632,674	484,838	81,586
No. of unique reflections	53,414	39,606	16,881
Completeness (%)	98.5 (82.7)	99.9 (99.7)	97.9 (96.5)
$\langle I/\sigma(I)\rangle$	41.5 (4.3)	26.6 (2.8)	12.3 (2.3)
R_{sym} (%)	4.9 (26.8)	10 (60.8)	12.5 (67.0)
Wilson B, Å^2/mosaic spread, °	26.0/0.3	46.3/0.3	26.7/0.8
Protein residues	388	385	383
Metal ions (number)	Zn^{2+} (2)	Zn^{2+} (2), Hg^{2+} (4)	Zn^{2+} (2)
Water/sulfate/fosfomycin molecules	547/15/–	460/8/–	244/–/2
R_{work}/R_{free}, %	18.8/23.0	18.1/24.2	18.3/27.0
Average thermal parameters, Å^2			
Subunit A/B overall	25.0/25.3	30.5/29.4	43.2/47.5
All main/side chain	23.0/27.4	27.8/32.1	44.3/46.4
Solvent/sulfate or fosfomycin	39.4/48.4	42.8/58.1	44.5/63.1
Metal ions (Zn^{2+}/Hg^{2+})	29.5	36.3/34.8	46.4
rms bond lengths, Å/bond angles, °	0.012/1.44	0.016/1.44	0.008/1.26
PDB ID code	2BNM	2BNN	2BNO

Numbers in parentheses correspond to the statistics for the highest-resolution bin.

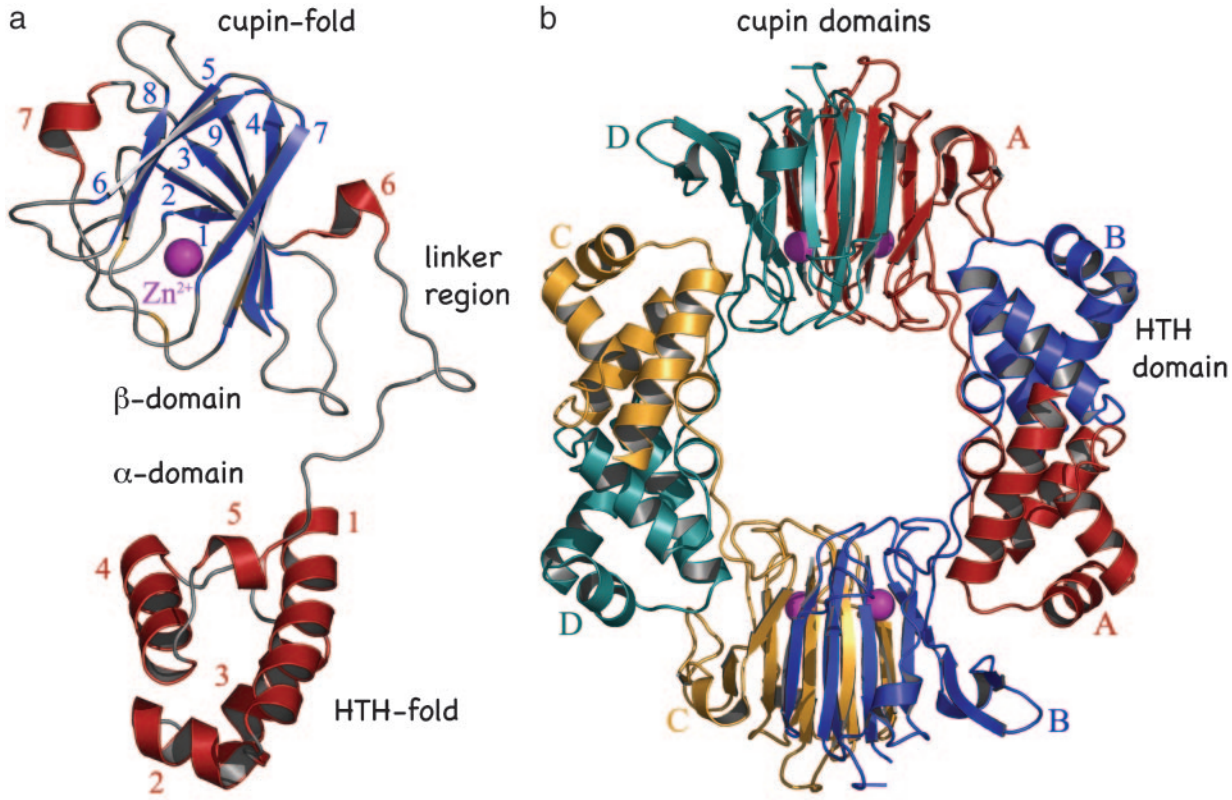

Fig. 2. Molecular structure. (*a*) Ribbon diagram of the HPPE subunit with α helices colored red and β strands, blue. Zn^{2+} is depicted as a sphere (magenta). (*b*) The functional tetramer viewed down a crystallographic twofold axis. Subunits are coloured red (A), blue (B), gold (C), and cyan (D). PYMOL (28) was used for molecular images.

7.9/50 mM NaCl was carried out on a UNICAM 939 spectrometer (Unicom Analytical Systems, Cambridge, U.K.) at wavelengths of 248.3 and 213.9 nm for Fe^{2+} and Zn^{2+}, respectively. Each lamp (for Fe and Zn) was set to 75% current, with an air/C_2H_2 flame and measurements taken at 4-sec intervals. Standards were prepared in the same buffer as protein by using 31.25, 62.5, and 125 nM $Fe(NH_4)_2(SO_4)_2$ and $ZnCl_2$. No Fe^{2+}, but only Zn^{2+}, at a concentration of $\approx$60 nM, was observed in recombinant HPPE. The highly efficient expression system (13) is therefore producing 80% apoenzyme (80%) and HPPE-Zn (20%). The addition of Zn^{2+} during crystallization produces a homogeneous holoenzyme sample. A previous study showed that recombinant HPPE did not contain any significant quantity of $Fe^{2+/3+}$, in agreement with our findings; however, no attempt to quantify Zn^{2+} is mentioned (9).

X-ray absorption near-edge structure scans at BM14 were carried out at the K-absorption edges of first-row transition metals and indicated the presence of Zn^{2+} with a very weak signal from Ni^{2+}, the latter likely due to residual ions carried over from the purification by metal ion affinity chromatography (13). Diffraction data were measured at the high-energy sides of the Ni^{2+} and Zn^{2+} K-absorption edges (λ = 1.476 and 1.272 Å respectively) to 2.0- and 1.7-Å resolution. The data collected at the Ni^{2+} edge had an R_{sym} = 4.7% and coverage of 98.5%, and the Zn^{2+}-edge data set is that of HPPE-Zn (Table 1). Anomalous difference Fourier calculations (not shown) were consistent with well defined Zn^{2+} in the active sites, with peak heights of 72σ with the Zn^{2+}-edge dataset (a factor of 10 above other peaks) and 17σ with the Ni^{2+}-edge dataset. In the longer-wavelength dataset, the anomalous signal from sulfur atoms gave peaks of 12σ. Hence the peaks observed in this data set are consistent with the theoretical anomalous dispersion contribution from Zn^{2+} and S, but not Ni^{2+}, at that wavelength.

Results and Discussion

The Structure of HPPE. Three structures have been determined (HPPE-Hg, the derivative used for structure solution, HPPE-Zn, and HPPE-Fos; Table 1). Because HPPE-Hg is highly similar to HPPE-Zn, although at reduced resolution, we detail only the 1.7-Å HPPE-Zn and 2.5-Å HPPE-Fos structures. The entire A and B subunits of HPPE-Zn are present in the model, with the exception of the four N-terminal residues, and the subunits overlay well with 186 residues having a rms deviation (rmsd) on Cα atoms of 0.52 Å. This is a noteworthy agreement, because subunits were treated independently during the analysis. Subunit A is mainly used in discussion. The HPPE-Zn and HPPE-Fos structures are similar (rmsd on Cα positions of 0.66 Å, excluding residues 94–103), except for the loop between β1 and β2, which will be detailed later.

The HPPE subunit, approximate mass 21 kDa, consists of two distinct domains joined by a 15-residue linker region (residues 72–86; Fig. 2*a*). The N-terminal or α domain (residues 5–71) consists of five helices (α1–5) that form a compact structure enclosing a hydrophobic, mainly aliphatic, core. The first helix, α1, is the longest, extending from residues 5 to 22. Helices α1-α2-α3 are connected by short segments of one or two residues, with the longest loop in this domain being seven residues long connecting α3 with α4. The shortest section of helix, α5, five residues in length, completes the domain. The C-terminal β domain, or catalytic domain, is a central β-barrel of nine strands, flanked by two short helices (α6 and α7). Helix α6 lies at the start of the barrel, just before β1. Strands β1 and β2 run antiparallel to each other, as do strands β4, β5, β6, β7,

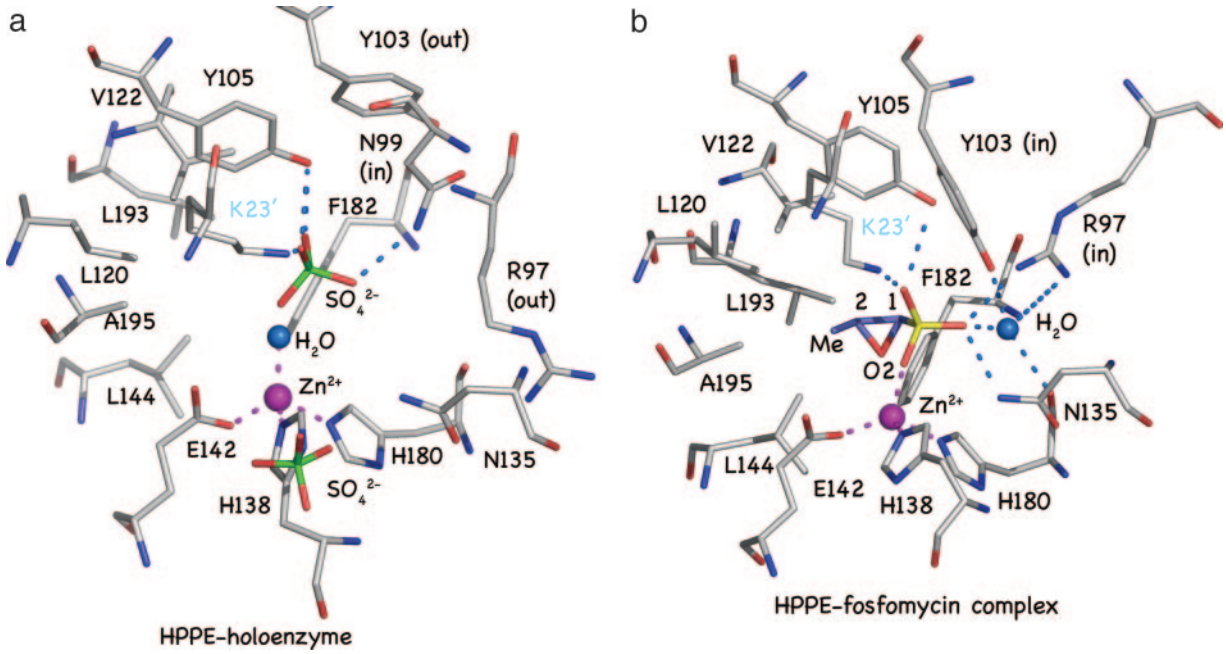

Fig. 3. The active site. (*a*) HPPE-Zn. (*b*) HPPE-Fos. Amino acids are shown in stick mode colored according to atom type (C, gray; N, blue; and O, red), the fosfomycin is colored C, slate blue; P, yellow; and sulfate S, green. Selected water molecules and Zn^{2+} ions are depicted as blue and magenta spheres, respectively. Magenta dashed lines represent coordination to the cation, and blue dashed lines selected hydrogen-bonding interactions. Tyr-105 binds sulfate/phosphonate groups and neither coordinates the active site metal nor shows any signs of covalent modification. The Lys-23 label is cyan to highlight that it is contributed from a partner subunit.

and β8. The missing residues in the structure of HPPE-Fos correspond to the loop between β1 and β2, in subunit B. The enzyme active site, detailed later, is located within the β-barrel of each catalytic domain and contains a well ordered Zn^{2+}.

Two subunits constitute the asymmetric unit, and a crystallographic twofold axis of symmetry generates the functional homotetramer (subunits A, B, C, and D) of approximate dimensions 81 × 64 × 38 Å (Fig. 2*b*). The tetramer, with 222-point group symmetry, is formed by the association of the α domains of subunits A and B (or C and D) and the interactions of the β domains from subunits A and D (or B and C). There are no contacts between subunits A and C, B and D. A large (25 × 29-Å) hole, occupied by water and eight sulfate ions, is formed within the tetramer.

The accessible surface area of subunit A is 11,925 Å^2, and this is reduced to 10,220, 10,270, and 8,570 Å^2 (14.3%, 13.9%, and 28.2% buried) when in contact with subunit B or D or as part of the complete tetramer, respectively. Some 51 residues and three sulfates contribute to the interface between subunits A and B. The protein residues are in secondary structural elements spanning: α1 to the N terminus of α2, the loop between α3 and α4 to the N terminus of the loop between α5 and α6, and β1 to β3. Eleven direct intersubunit hydrogen bonds are involved in this association. The interface between subunits A and D is an association of β domains involving 43 residues on strands β2–β6, β9, and the loop between β7 and β8, with 22 direct hydrogen bonds contributing to this interface.

Structural Homologues. Architectural comparisons with known structures (20) revealed that HPPE constitutes a unique combination of domains. The α domain matches closely to helix–turn–helix (HTH) DNA-binding proteins, in particular the N-terminal domain of 434 repressor [ref. 21; Protein Data Bank (PDB) ID code 1R69; *z* score 10.4] and the tetrameric repressor SinR (ref. 22; PDB ID code 1B0N; *z* score 9.7). The *z* score is a measure of the statistical significance of the best domain–domain alignment (20). Typically, dissimilar proteins will have a *z* score of <2.0, and subunit A matched with itself gives a *z* score of 28. The α domain aligned with 61 and 66 residues of these HTH proteins providing rms deviations on Cα positions of 1.4 and 2.1 Å, respectively. Secondary structure matching[‖] revealed that ≈80% of the secondary structural elements of the α domain and homologues aligned well.

The HTH motif is responsible for sequence-specific DNA binding and typically occurs in repressors and transcriptional regulators (23). The HTH motif refers to two helices (α2 and α3 in HPPE) separated by a tight β turn. In HTH–DNA complexes, the second α helix, or recognition helix, binds in the major groove of DNA, making sequence-specific interactions. HTH proteins are dimeric, and two recognition helices lie in the correct orientation (≈34 Å apart, equivalent to one turn of duplex DNA) to mediate protein–DNA interactions. In HPPE, α3 from subunit A is ≈34 Å from α3 of subunit B, and structural overlays with the HTH proteins (not shown) suggest that HPPE might indeed bind DNA. Moreover, consideration of the primary sequences (not shown) shows strong conservation of four residues important for DNA binding. These residues correspond to HPPE Lys-16, Arg-19, His-26, and Asn-45. In the 434-repressor, these residues are Lys-7, Arg-10, Gln-17, and Asn-36. In addition, DNA-binding HTH proteins contain a highly conserved buried Arg-Glu salt bridge important for the integrity of the domain structure (24). In HPPE, this electrostatic association is conserved between Arg-19 and Glu-44 (not shown). Intriguing though this structural relationship between the HPPE α domain and HTH proteins is, there is as yet no evidence that HPPE does, in fact, bind DNA.

The catalytic β domain corresponds to the cupin superfamily fold, so named because of the characteristic β barrel shape (ref. 25; *cupa*, Latin for barrel). The closest structural homologues are

[‖]Krissinel, E. & Henrick, K., 5th International Conference on Molecular Structural Biology, eds. Kungl, A. J. & Kungl, P. J., Sept. 3–7, 2003, Vienna.

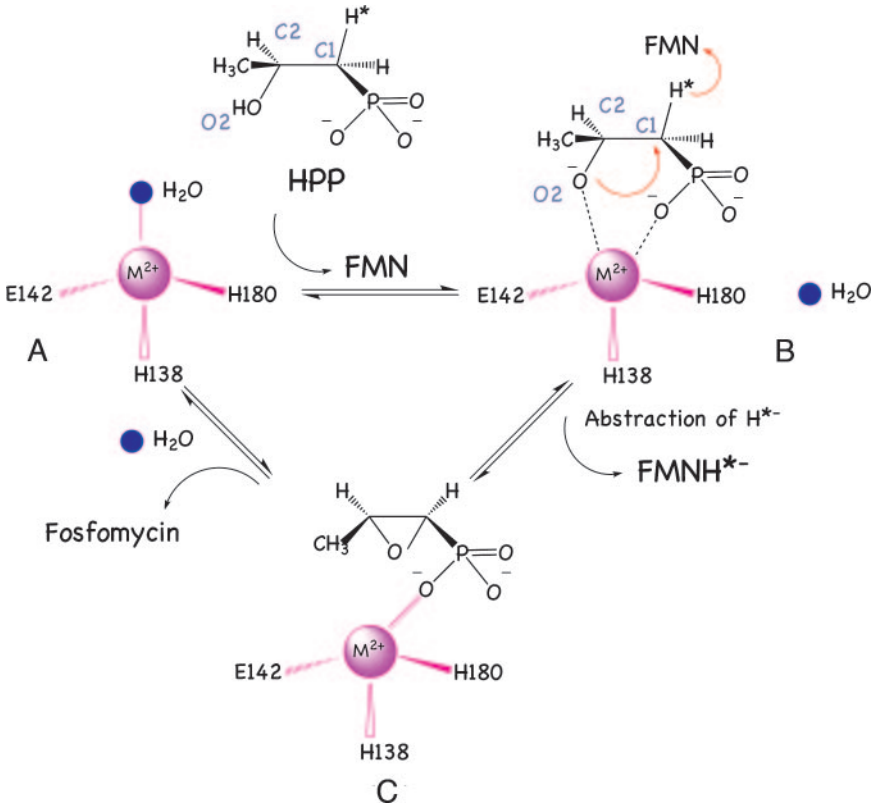

Fig. 4. A postulated mechanism for HPPE. States A and C are represented by the structures HPPE-Zn and HPPE-Fos, respectively.

a manganese-containing cupin of unknown function (Tm1459) (ref. 26; PDB ID code 1VJ2, *z* score 12.6) and the archetypal family member, germin (ref. 27, PDB ID code 1FI2, *z* score 9.8). The β domain aligned with 106 residues of both Tm1459 and germin, with rms deviations of 2.8, and 3.5 Å, respectively. As with the HTH domain, ≈80% of secondary structural elements of the β domain, in particular β strands 2–9 of HPPE, overlay well with the corresponding strands in other cupins.

The Active Site. The catalytic site lies within the β barrel (Figs. 2 and 3), where Zn^{2+} binds with tetrahedral coordination to His-138-NE2, Glu-142-OE1 (*syn*-monodentate), His-180-NE2, and a water molecule. The coordinating water forms hydrogen bonds with other water molecules (not shown) that coordinate a sulfate, which in turn interacts with Tyr-105-OH, Asn-99-ND2, and also Lys-23′ from subunit B (′ signifies the partner subunit; Fig. 3*a*). Lys-23′ is flexible and displays discrete rotamers, one of which interacts with this sulfate. Hydrophobic side chains (Val-118, Leu-120, Leu-144, Phe-182, Leu-193, and Ala-195) line one side of and also create the floor of the active site. Mainly hydrophilic side chains (Lys-23′, Arg-97, Asn-99, Tyr-103, Tyr-105, Asn-135, His-138, Glu-142, and His-180) and Zn^{2+} constitute the remainder of the active site and bind numerous well ordered water molecules (not shown).

In HPPE-Fos, the antibiotic product displaces both the water molecule that coordinates Zn^{2+} and the nearby sulfate ion. The coordination of Zn^{2+} by the enzyme is retained, but there is a rotation of the side chain of His-138 to accommodate interactions with a sulfate different from that discussed above (Fig. 3). Tetrahedral coordination is achieved by interacting with a phosphonate oxygen of the antibiotic, whereas the epoxide oxygen is ≈2.8 Å distant from the cation. The phosphonate group accepts hydrogen bonds donated from Arg-97-NH2, Tyr-105-OH, and Asn-135-ND2 from one subunit, along with Lys-23′, and a well ordered water molecule.

The residues that bind fosfomycin are mainly involved in binding a sulfate in HPPE-Zn, either directly or through mediating water molecules. However, when fosfomycin binds, Tyr-103 and Arg-97 swing in toward the catalytic center, whereas Asn-99 is directed out of the active site (Fig. 3). The tyrosine hydroxyl binds the phosphonate directly and the arginine participates in a solvent-mediated interaction with the antibiotic. This exchange of residues in the active site results from a conformational change (parts of Arg-97 and Asn-99 move almost 10 Å) in the loop between β1 and β2. In HPPE-Zn, the loop, which includes a flexible Gly-95, forms the interface between the β domain of subunit A and the α domain of subunit B. When the product is present, the loop has adjusted position to create a gap between the two subunits. As the Cα positions of the loop move away from subunit B and toward the solvent, several side chains (Tyr-103 and Tyr-105, for example) move into the active site area, resulting in a smaller binding pocket for fosfomycin (Fig. 3).

Enzyme Activity and Mechanism. Bioautograph assays indicate that apo-HPPE is inactive and Zn^{2+}- and Fe^{2+}-containing HPPE samples are active, produce fosfomycin, and inhibit bacterial growth in the presence of FMN. Recombinant HPPE, which contains only 20% of Zn^{2+}-holoenzyme, has a catalytic productivity, i.e., maximal level of fosfomycin produced, of 1.5 μg under our assay conditions. The most active enzyme, productivity of 4.5 μg, is the reconstituted HPPE-Fe, with lower productivity of 1.5 μg observed for the Zn^{2+} reconstituted protein. Because only 20% of the total recombinant protein before EDTA treatment and metal ion reconstitution used in the assays is HPPE-Zn, then it displays a comparable level of activity to the Fe^{2+}-reconstituted HPPE, but reconstitution with Zn^{2+} does not increase the activity 5-fold. It is unclear whether EDTA treat-

ment has any deleterious effect on the protein structure that might influence subsequent reconstitution with divalent cations.

The critical observation is that HPPE-Zn, like HPPE-Fe, is active. The metal ions have similar size (ionic radii 0.75 and 0.77 Å, respectively) and chemical properties. The significant difference is that Zn^{2+} is redox inert, and this rules out metal ion redox chemistry as a requirement for activity; rather, it is the strong Lewis acid characteristics of the cations that contribute to the mechanism. Other metal ions do not facilitate HPPE activity (8). The smaller ionic radius of Ni^{2+}, for example (0.69 Å), has steric implications, which, combined with differences in coordination preferences and the weaker Lewis acid properties compared with Zn^{2+}/Fe^{2+}, suggests why this cation does not support catalysis. Although a crystal structure of HPPE in complex with FMN has so far eluded our determined efforts, calorimetric data confirm stoichiometric binding with a K_d of $\approx$10 μM. This information, in concert with the structures, suggests the following mechanism, which can be broken down into three states (states A–C, Fig. 4).

In state A, a water molecule coordinates the Lewis acid M^{2+}. Polarization may produce hydroxide, which could abstract a proton from the O2 hydroxyl group as substrate binds. More likely is that the substrate binds and displaces the coordinating water with the phosphonate and O2 hydroxyl, generating a five-coordinate transition state complex, state B. The substrate hydroxyl would be activated with the nearby Glu-142-OE1 placed to acquire the O2 proton producing an alkoxide. A cationic species is generated as FMN abstracts the hydrogen atom H* stereospecifically as a hydride ion from C1. The O2 alkoxide attacks C1 from the opposite side of H* abstraction and forms the C1—O2 bond with inversion of configuration. This gives the major product fosfomycin by a mechanism, consistent with previous findings (7). A very minor product (not depicted) is the trans-epoxide, which would be generated after rotation (180°) about the C1—C2 bond (7). The structural differences between HPPE-Zn and HPPE-Fos and the stereochemistry of the reaction are consistent with the hypothesis that FMN would bind over toward Tyr-103, Arg-97, Asn-99, and the flexible loop discussed earlier. A degree of conformational freedom would assist the release of product, with water again binding to the metal ion to maintain tetrahedral coordination.

We thank M. Alphey, C. Bond, N. Ramsden, and D. Wilson for advice and the European Synchrotron Radiation Facility for access. This work was funded by the Biotechnology and Biological Sciences Research Council and the Wellcome Trust.

1. Hendlin, D., Stapley, E. O., Jackson, M., Wallick, H., Miller, A. K., Wolf, F. J., Miller T. W., Chaiet, L., Kahan, F. M., Foltz, E. L., *et al.* (1969) *Science* **166,** 122–123.
2. Katz, A. H. & Caufield, C. E. (2003) *Curr. Pharmacol. Des.* **9,** 857–866.
3. Hidaka, T., Goda, M., Kuzuyama, T., Takei, N., Hidaka, M. & Seto, H. (1995) *Mol. Gen. Genet.* **249,** 274–280.
4. Seto, H. & Kuzuyama, T. (1999) *Nat. Prod. Rep.* **16,** 589–596.
5. Hammerschmidt, F. & Kaehlig, H. (1991) *J. Org. Chem.* **56,** 2364–2370.
6. El Zoeiby, A., Sanschagrin, F. & Levesque, R. C. (2003) *Mol. Microbiol.* **47,** 1–12.
7. Woschek, A., Wuggenig, F., Peti, W. & Hammerschmidt, F. (2002) *ChemBioChem* **3,** 829–835.
8. Liu, P., Liu, A., Yan, F., Wolfe, M. D., Lipscomb, J. D. & Liu, H. W. (2003) *Biochemistry* **42,** 11577–11586.
9. Liu, P., Mehn, M. P., Yan, F., Zhao, Z., Que, L., Jr., & Liu, H. W. (2004) *J. Am. Chem. Soc.* **126,** 10306–10312.
10. Costas, M., Mehn, M. P., Jensen, M. P. & Que, L., Jr. (2004) *Chem. Rev.* **104,** 939–986.
11. Hausinger, R. (2004) *Crit. Rev. Biochem. Mol. Biol.* **39,** 21–68.
12. Archelas, A. & Furstoss, R. (1997) *Annu. Rev. Microbiol.* **51,** 491–525.
13. Cameron, S., McLuskey, K., Chamberlayne, R., Hallyburton, I. & Hunter, W. N. (2005) *Acta Crystallogr. F* **61,** 534–536.
14. Otwinowski, Z. & Minor, W. (1997) *Methods Enzymol.* **276,** 307–326.
15. Collaborative Computational Project, Number 4. (1994) *Acta Crystallogr. D* **50,** 760–763.
16. Terwilliger, T. C. (2003) *Methods Enzymol.* **374,** 22–37.
17. Perrakis, A., Morris, R. & Lamzin, V. S. (1999) *Nat. Struct. Biol.* **6,** 458–463.
18. Jones, T. A., Zou, J. Y., Cowan, S. W. & Kjeldgaard. (1991) *Acta Crystallogr. A* **47,** 110–119.
19. Murshudov, G. N., Vagin, A. A., Lebedev, A., Wilson, K. S. & Dodson, E. J. (1999) *Acta Crystallogr. D* **55,** 247–255.
20. Holm, L. & Sander, C. (1995) *Trends. Biochem. Sci.* **20,** 478–480.
21. Mondragon, A., Subbiah, S., Almo, S. C., Drottar, M. & Harrison, S. C. (1989) *J. Mol. Biol.* **205,** 189–200.
22. Lewis, R. J., Brannigan, J. A., Offen, W. A., Smith, I. & Wilkinson, A. J. (1998) *J. Mol. Biol.* **283,** 907–912.
23. Brennan, R. G. & Matthews, B. W. (1989) *J. Biol. Chem.* **264,** 1903–1906.
24. Pervushin, K., Billeter, M., Siegal, G. & Wuthrich, K. (1996) *J. Mol. Biol.* **264,** 1002–1012.
25. Dunwell, J. M., Purvis, A. & Khuri, S. (2004) *Phytochemistry* **65,** 7–17.
26. Jaroszewski, L., Schwarzenbacher, R., von Delft, F., McMullan, D., Brinen, L. S., Canaves, J. M., Dai, X., Deacon, A. M., DiDonato, M., Elsliger, M. A., *et al.* (2004) *Proteins* **56,** 611–614.
27. Woo, E. J., Dunwell, J. M., Goodenough, P. W., Marvier, A. C. & Pickersgill, R. W. (2000) *Nat. Struct. Biol.* **7,** 1036–1040.
28. DeLano, W. L. (2002) *The PyMOL Molecular Graphics System* (DeLano Scientific, San Carlos, CA).